

Article

Ultraviolet Upconversion Emission of $\text{CaAl}_2\text{SiO}_6$ Polycrystals Doped with Pr^{3+} Ions

Karol Lemański , Nadiia Rebrova , Patrycja Zdeb-Stańczykowska  and Przemysław Jacek Dereń 

Institute of Low Temperature and Structure Research, Polish Academy of Sciences, ul. Okólna 2, 50-422 Wrocław, Poland; n.rebrova@intibs.pl (N.R.); p.zdeb@intibs.pl (P.Z.-S.); p.deren@intibs.pl (P.J.D.)

* Correspondence: k.lemanski@intibs.pl

Abstract

The spectroscopic properties of Pr^{3+} ions in the aluminosilicate matrix were investigated for the first time. Synthesis of $\text{CaAl}_2\text{SiO}_6$ (CASO) polycrystals doped with Pr^{3+} ions was carried out using the sol–gel method. The crystalline structures have been confirmed with XRD measurement. The absorption, excitation, emission spectra, and time decay profiles of the praseodymium (III) ions were measured and analyzed. It was found that upon excitation with visible light, this material exhibits emission mainly in the UVC region, via an upconversion emission process. The Stokes emission in the visible range is observed mainly from the $^3\text{P}_0$ and $^1\text{D}_2$ energy levels. The $^1\text{D}_2 \rightarrow ^3\text{H}_4$ emission is very stable even at very high temperatures. The studied aluminosilicate phosphors possess characteristics that confirm their potential in upconversion emission applications.

Keywords: luminescence; UVC; praseodymium; upconversion; polycrystals; aluminosilicates; spectroscopy



Academic Editor: Igor Reva

Received: 4 June 2025

Revised: 4 July 2025

Accepted: 9 July 2025

Published: 11 July 2025

Citation: Lemański, K.; Rebrova, N.; Zdeb-Stańczykowska, P.; Dereń, P.J. Ultraviolet Upconversion Emission of $\text{CaAl}_2\text{SiO}_6$ Polycrystals Doped with Pr^{3+} Ions. *Molecules* **2025**, *30*, 2944. <https://doi.org/10.3390/molecules30142944>

Copyright: © 2025 by the authors. Licensee MDPI, Basel, Switzerland. This article is an open access article distributed under the terms and conditions of the Creative Commons Attribution (CC BY) license (<https://creativecommons.org/licenses/by/4.0/>).

1. Introduction

The phenomenon of upconversion emission was first described by N. Bloembergen [1] and soon after by F. Auzel [2]. There are various upconversion mechanisms [3,4]. The probability of their occurrence is different, which is why their efficiency and frequency of occurrence are different. Most publications related to this phenomenon concern the conversion of infrared radiation into visible light, where Er^{3+} - Yb^{3+} [5,6] or possibly Ho^{3+} - Yb^{3+} [5,7], Tm^{3+} - Yb^{3+} [8], Tb^{3+} - Yb^{3+} [9], and also Pr^{3+} - Yb^{3+} [10,11] ions are usually used, due to the appropriate matching of the energy levels of electrons on the 4f subshell and the effective energy transfer from Yb^{3+} ions to other lanthanide ions. This process can also concern the conversion of visible light, e.g., blue, into high-energy radiation in the ultraviolet range. This creates additional application possibilities due to the disinfecting properties of UV radiation, which destroys viruses and bacteria; mainly UVC [12] but also UVB [13] and even UVA [14,15] could be used for disinfection purposes.

Praseodymium ions are good candidates for various applications in the luminescence field, to generate visible light [16–18], and also for emitting UV radiation from the 5d level in suitable matrices [19,20], because this level is at a large distance from the lower levels, such as $^3\text{P}_j$, so luminescence quenching via multiphonon relaxation processes [21,22] will not occur, even for matrices with high phonon energy. Not all luminescent materials are good candidates for generating UV radiation through the upconversion processes, especially in the high-energy UVC region (100–280 nm), which destroys germs. Effective

UVC radiation for the Pr^{3+} -doped samples, induced by the upconversion process, should occur from the 5d level of Pr^{3+} ions; therefore, the energy bandgap of these materials should be large enough for the 5d level to be situated inside this energy bandgap, not in the conduction band. The 5d-4f emission is allowed by the selection rule transition, so it will be characterized by good intensity and a short emission lifetime. The threat for efficient emission from the 5d level is the high 4f energy level $^1\text{S}_0$, which, depending on the crystal matrix, is located inside the 5d band or slightly below this band, because the location of the 5d band can be different for the different hosts. Aluminosilicate $\text{CaAl}_2\text{SiO}_6$ is a good matrix for potentially efficient upconversion emission in the UVC region, because it has a high value of the energy bandgap, and also because the $^1\text{S}_0$ multiplet is located above the minimum of the 5d band, so there will be no parasitic quenching processes of this emission in this case.

The investigated aluminosilicate $\text{CaAl}_2\text{SiO}_6$ has a sufficiently large energy bandgap, which will be described in detail later in the text. Moreover, it also has a $^1\text{S}_0$ level located inside the 5d band, so it is a suitable candidate for obtaining efficient upconversion of emission in the UVC region. $\text{CaAl}_2\text{SiO}_6$ Yoshiokaite mineral structure was first collected from the Moon by the Apollo 14 crew in 1971 [23]. In the scientific literature, there are some papers describing the luminescent properties of $\text{CaAl}_2\text{SiO}_6$ [24–28], but still not all lanthanides have been doped into this host to check its spectroscopic characteristics.

In this work, we present novel results on the luminescent properties of Pr^{3+} ions in the aluminosilicate matrix $\text{CaAl}_2\text{SiO}_6$. Particular attention was given to the results concerning the rarely recorded conversion of visible light to emission in the UVC region.

2. Results and Discussion

The exact formula of the Yoshiokaite structure of the studied aluminosilicate is $\text{Ca}_{5.35}\text{Al}_{10.7}\text{Si}_{5.3}\text{O}_{32}$ [29]. Crystals possess a P-3 (147) trigonal space group, where the ICDD (International Centre for Diffraction Data) code is 01-080-1547 (Figure 1), and the corresponding number of the ICSD (Inorganic Crystal Structure Database) is 69380. Details regarding the structural properties of CASO aluminosilicate were given in a previously published work [25]; however, after a more detailed structural analysis, it was found that Ca^{2+} ions are coordinated by nine oxygen ions, where the bond length of each $\text{Ca}^{2+}\text{-O}^{2-}$ pair is equal to 2.375, 2.413, 2.417, 2.482, 2.492, 2.718, 2.726, 2.920, 2.921 [Å]. The ionic radius of Ca^{2+} ions in the coordination of IX ligands is equal to 1.32 Å [30]. The radius of Pr^{3+} ions (1.319 Å) perfectly matches the ionic size of Ca^{2+} in this coordination.

The obtained diffractograms confirm the structure of the tested aluminosilicate for all samples (Figure 2). A slight, broad band with a center at about 15 degrees for the sample with the smallest amount of impurity, 0.1% Pr^{3+} , indicates a slight share of the amorphous phase in the composition of this sample. The diffraction patterns of the investigated crystalline powders correspond to the standard from the crystallographic database with the number ICDD 00-080-1547.

The W-H analysis was performed by plotting $4\sin\theta$ on the x -axis against $\beta\cos\theta$ on the y -axis for the six most intense diffraction peaks, as shown in Figure 3. The crystallite size and lattice strain were determined from the y -intercept and slope of the linear fit, respectively (Table 1). It should be noted that there is no observable dependence of crystallite size and lattice strain on the activator concentration.

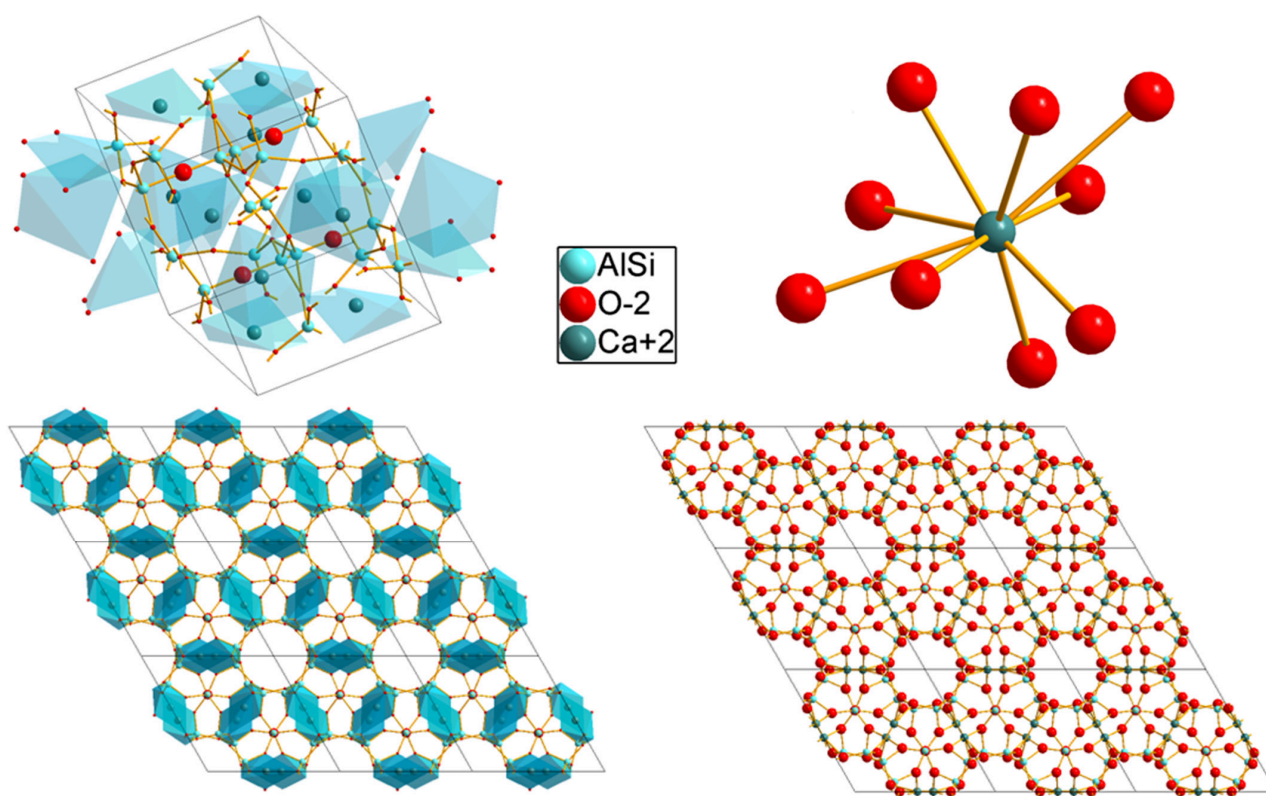


Figure 1. Visualization of the investigated aluminosilicate crystal structure (ICDD 01-080-1547).

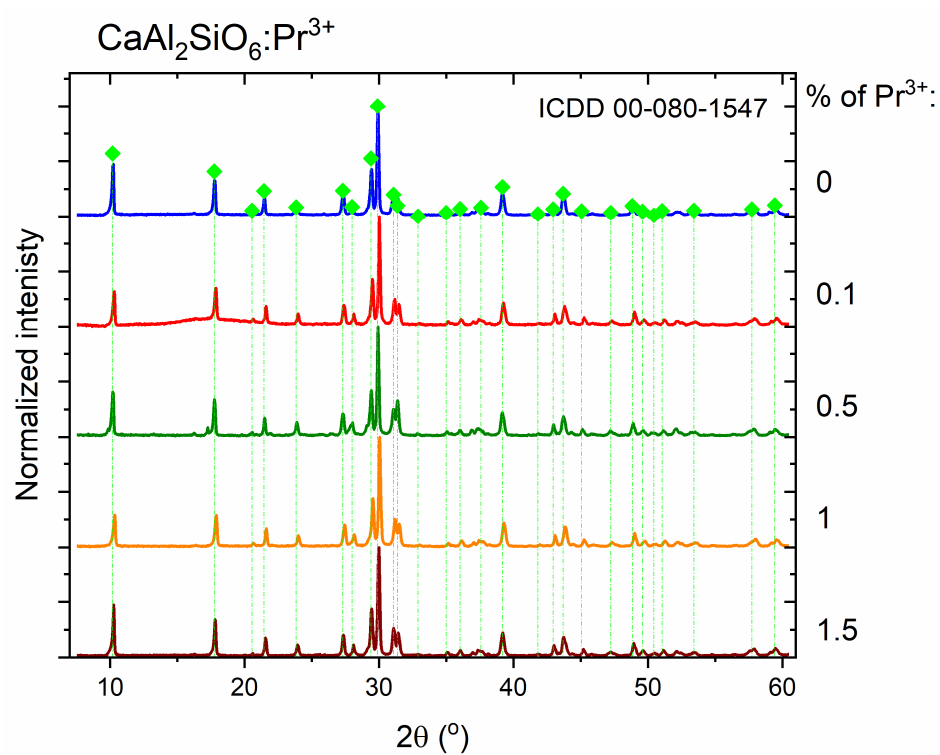


Figure 2. XRD patterns of the measured polycrystals of $\text{CaAl}_2\text{SiO}_6$.

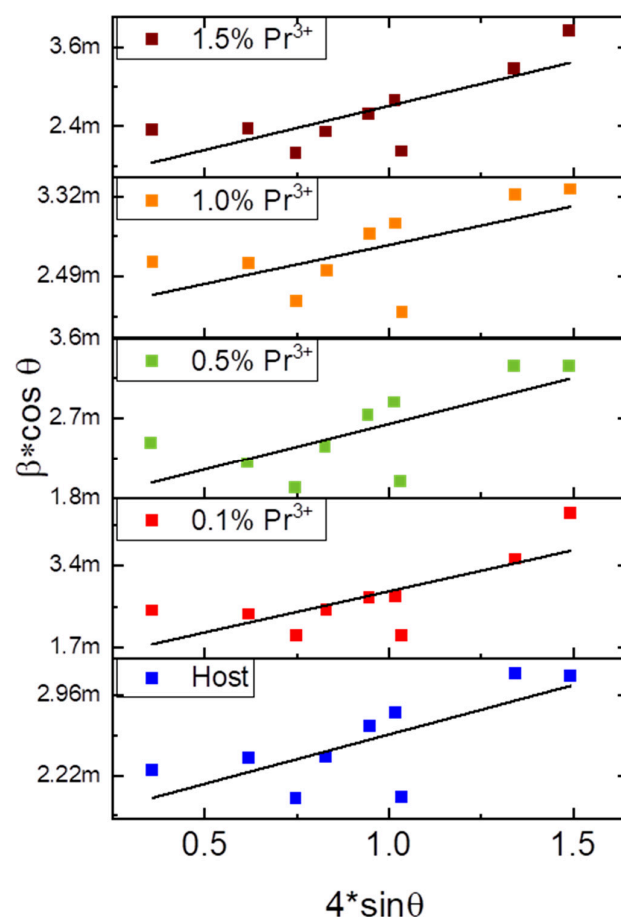


Figure 3. Plots of $b \cdot \cos \theta$ versus $4 \cdot \sin \theta$ for $\text{CaAl}_2\text{SiO}_6$ and $\text{CaAl}_2\text{SiO}_6:\text{Pr}^{3+}$ particles.

Table 1. Lattice parameters, unit cell volume and calculated crystallite size of $\text{CaAl}_2\text{SiO}_6:\text{Pr}^{3+}$ particles.

Sample	Lattice Parameters			Crystallite Size		Strain $\times 10^{-3}$
	a (Å)	c (Å)	V (Å ³)	SM (nm)	W-H (nm)	
$\text{CaAl}_2\text{SiO}_6$	9.9278	8.2172	701.39	68.8	82.0	1.33
$\text{CaAl}_2\text{SiO}_6:0.1\%\text{Pr}^{3+}$	9.9288	8.2397	703.46	71.3	119.5	0.81
$\text{CaAl}_2\text{SiO}_6:0.5\%\text{Pr}^{3+}$	9.9429	8.2325	704.84	70.3	86.6	1.04
$\text{CaAl}_2\text{SiO}_6:1.0\%\text{Pr}^{3+}$	9.9562	8.2394	707.32	65.6	70.9	1.71
$\text{CaAl}_2\text{SiO}_6:1.5\%\text{Pr}^{3+}$	9.962	8.2613	710.02	68.9	101.2	0.91

With an increase in the concentration of doped Pr^{3+} ions and charge-compensating Na^+ ions, there is a slight increase in the crystal lattice parameters (Table 1), which may be caused by the expansion of the volume of unit cells by the influence of larger sodium ions (Na^+), whose ionic radius is 1.38 Å, which is larger than the radius of Ca^{2+} ions (1.32 Å). Based on the X-ray diffraction data, the crystallite size of particles was estimated using the Williamson–Hall (W-H) [31] plot and Scherrer method (SM) [32]. Since the SM does not account for deformations and lattice defects, the average particle size calculated by this method is smaller (~70 nm) compared to the particle size estimated by the W-H method (~90 nm).

For the chemical compound $\text{CaAl}_2\text{SiO}_6$, the energy gap size was previously estimated using the method based on the chemical formula of an inorganic compound [26,33,34]. According to the calculation presented in the recently published paper, the energy bandgap $E_g = 7.68 \pm 0.20$ eV [26]. The size of the bandgap is large enough to accommodate the 5d

level of Pr^{3+} ions. The $^1\text{S}_0$ level is usually in the range of $46,000\text{--}47,000\text{ cm}^{-1}$ (217–213 nm), which in electron volts corresponds to a size of 5.70–5.83 eV, so this level also falls within the energy bandgap region.

Figure 4a shows the excitation and Stokes emission spectra for a selected $\text{CaAl}_2\text{SiO}_6$ sample doped with Pr^{3+} ions. In order to precisely conduct studies in the ultraviolet range, measurements of the polycrystalline powder were performed using LiF glass, which is also transparent in the UV range. Measurements using non-synthetic quartz could be slightly disturbed by its absorption band in this range. The figure above shows the luminescence spectrum at excitation in the 4f–5d band at 234 nm. The emission spectrum of the 5d→4f band, centered at about 268 nm, is already very close to the excitation line, because it starts at about 250 nm. This band disappears in the visible region, at about 380 nm. The emission peaks from the $^3\text{P}_0$ and $^1\text{D}_2$ levels are much less intense. This indicates that the vast majority of the excitation energy is transferred directly to the 5d band, which does not lose much of this energy for transfer to the 4f praseodymium levels, because the $^1\text{S}_0$ f-electron state is located above the lowest 5d state of the Pr^{3+} ions in this host. The wide energy range of the 5d level covers the $^1\text{S}_0$ energy level. Thanks to this, the majority of the energy transferred to the 5d level is converted to the luminescence coming from this level, not non-radiatively to the $^1\text{S}_0$ level. Therefore, the UVC emission from the 5d level of Pr^{3+} ions in the $\text{CaAl}_2\text{SiO}_6$ matrix is much more efficient.

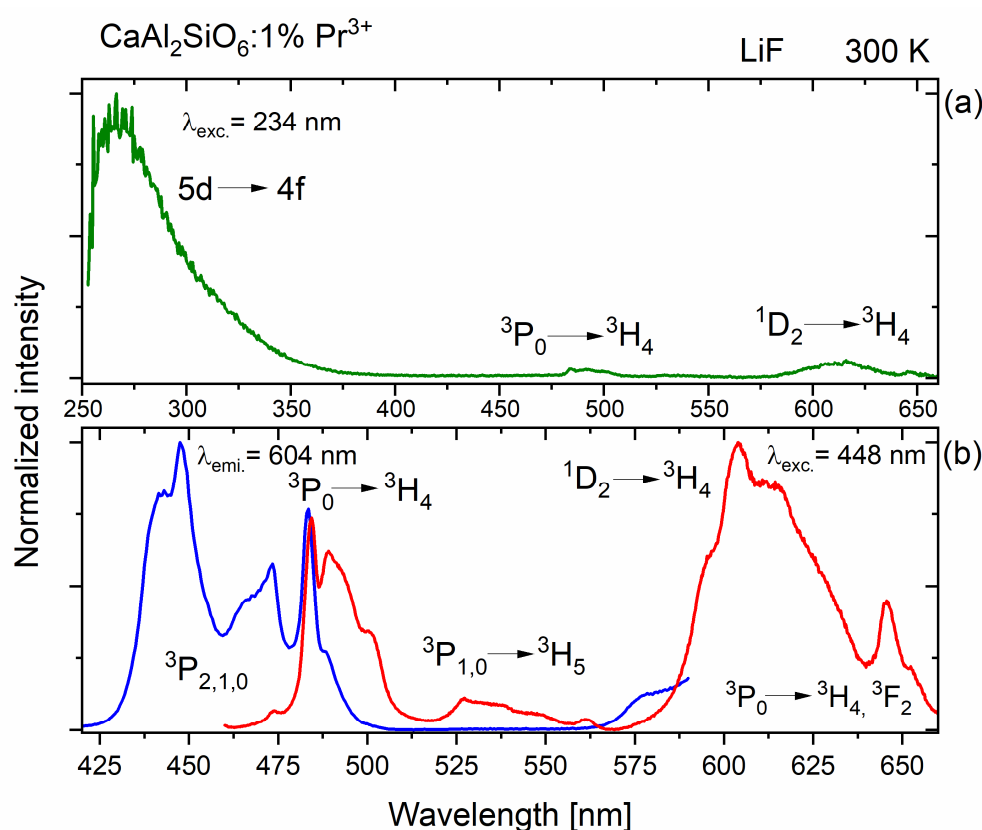


Figure 4. (a) 5d→4f emission spectrum of $\text{CaAl}_2\text{SiO}_6:\text{Pr}^{3+}$ for $\lambda_{\text{exc.}} = 234 \text{ nm}$; (b) 4f→4f excitation and emission spectra of $\text{CaAl}_2\text{SiO}_6:\text{Pr}^{3+}$ for $\lambda_{\text{exc.}} = 448 \text{ nm}$ and $\lambda_{\text{emi.}} = 604 \text{ nm}$.

In Figure 4b, the emission spectrum is presented, excited by a xenon lamp operating at a wavelength of 448 nm, matched to the Pr^{3+} level in the studied CASO matrix. This spectrum (red) is distributed over the excitation spectrum (blue), which is emitted when monitoring the emission at a wavelength of 604 nm, which defines the emission limits for

$^1D_2 \rightarrow ^3H_4$ transitions. The visible 3P_0 markings in these spectra are coincident with each other (Figure 4).

The emission bandwidth in the range of about 580–680 nm is quite significant. The most significant emission comes from the 1D_2 level, but in a similar range, there may also be a $^3P_0 \rightarrow ^3H_6$ transition, which partially overlaps with the $^1D_2 \rightarrow ^3H_4$ emission. By using a femtosecond laser and a streak camera, it was possible to perform time-resolved measurements and separate these spectra.

Figure 5 shows an image obtained directly from the streak camera, with visible areas reflecting the luminescence intensity. The X-axis shows the wavelength region on the nanometer scale. The Y-axis shows time in microseconds. In addition to the short-lived luminescence from the 3P_0 level, there is also visible longer-lived emission from the 1D_2 energy level.

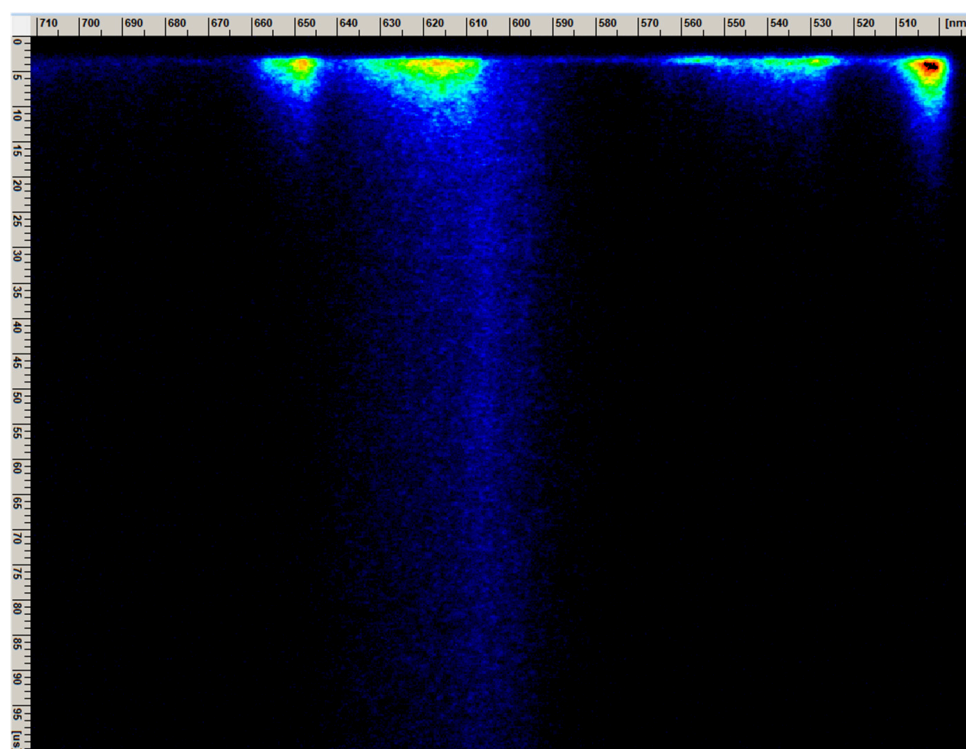


Figure 5. The image from the streak camera of $\text{CaAl}_2\text{SiO}_6:\text{Pr}^{3+}$, visualizing the short- and longer-living emission from 3P_1 and 1D_2 energy levels, respectively (Y-axis represents time in μs and X-axis represents wavelength in nm).

The emission spectrum of $\text{CASO}:\text{Pr}^{3+}$ (see Figure 6) was obtained from the measurements using a femtosecond laser streak camera, based on Figure 5, by using the program for processing spectra. In Figure 6, the blue color indicates the emission from the short-lived 3P_0 (part) and 3P_1 levels, while the red color indicates the longer-lived, spin-forbidden emission from the 1D_2 level. (The streak camera covered an incomplete portion of the visible spectrum, so the $^3P_0 \rightarrow ^3H_4$ transition was only partially shown.) It is clearly visible that the $^3P_0 \rightarrow ^3H_6$ and $^1D_2 \rightarrow ^3H_4$ emissions overlap, which is commonly found in the luminescence of Pr^{3+} ions. By measuring the luminescence decay times or time-resolved spectra (Figure 6), it is possible to separate these emissions.

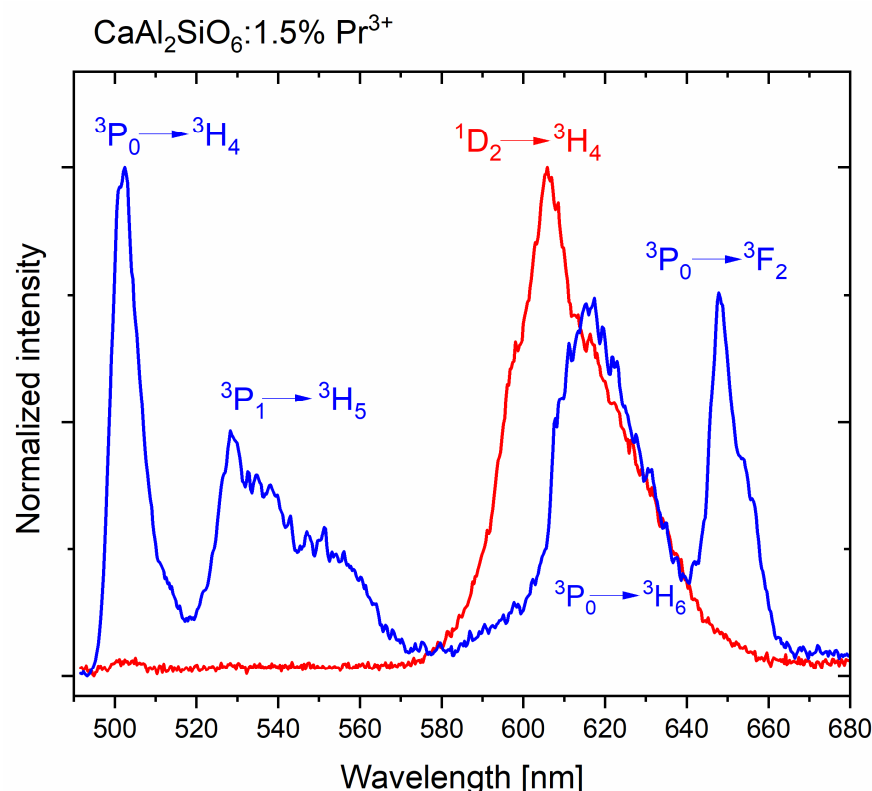


Figure 6. Emission spectra obtained from the streak camera of a femtosecond laser, with the separated emission from $^3\text{P}_J$ and $^1\text{D}_2$ levels of $\text{CaAl}_2\text{SiO}_6:\text{Pr}^{3+}$.

Figure 7 shows the dependence of praseodymium (III) emission in CASO polycrystals for the visible range, depending on the temperature. The main luminescence from the $^1\text{D}_2$ level to the ground state $^3\text{H}_4$ does not completely quench, even at a very high temperature of 500 °C, and retains over 40% of its highest intensity recorded for −175 °C, while the emission from the $^3\text{P}_0$ level is almost completely extinguished (see Figure 7). Moreover, it is interesting that the decrease in emission intensity possesses abnormal characteristics, due to the certain increase in the temperature range of 275–450 °C, where the maximum of this increase is for the temperature of 375 °C, which on the energy scale corresponds to the value of 450 cm^{-1} . A probable explanation for this phenomenon is the intensification of cross-relaxation processes according to the scheme $(^3\text{P}_1, ^3\text{H}_4) \rightarrow (^1\text{D}_2, ^3\text{H}_6)$, due to the appropriate energetic matching of these levels. This is because the increased temperature allows for a larger population of electrons in the $^3\text{P}_0$ excited state to reach the slightly higher energy of the $^3\text{P}_1$ level. Looking back at the excitation spectrum for $\text{CaAl}_2\text{SiO}_6:\text{Pr}^{3+}$ (see Figure 4), the $^3\text{H}_4 \rightarrow ^3\text{P}_0$ excitation peak has a maximum at 483 nm, which corresponds to an energy value of 20,704 cm^{-1} .

On the other hand, the $^3\text{H}_4 \rightarrow ^3\text{P}_1$ transition was recorded at a wavelength of 473 nm (i.e., 21,142 cm^{-1}). Therefore, it can be assumed that the energy difference between these levels is 438 cm^{-1} ; thus, it is almost resonantly matched to the temperature of 375 °C (450 cm^{-1}), for which there is a significant increase in the occupancy of the $^3\text{P}_1$ level from the $^3\text{P}_0$ level. Therefore, the above-mentioned cross-relaxations occur, which additionally occupy the $^1\text{D}_2$ energy level; thus, the emission from this level increases. Moreover, for this higher temperature, the $^1\text{D}_2$ level could be additionally occupied from the $^3\text{P}_0$ level by the multiphonon relaxation process. For higher temperatures, the cross-relaxation process $(^1\text{D}_2, ^3\text{H}_4) \rightarrow (^1\text{G}_4, ^3\text{F}_4)$ which quenches the emission from the $^1\text{D}_2$ level [35] is more probable, due to the better energy matching for the phonon-assisted cross-relaxation process.

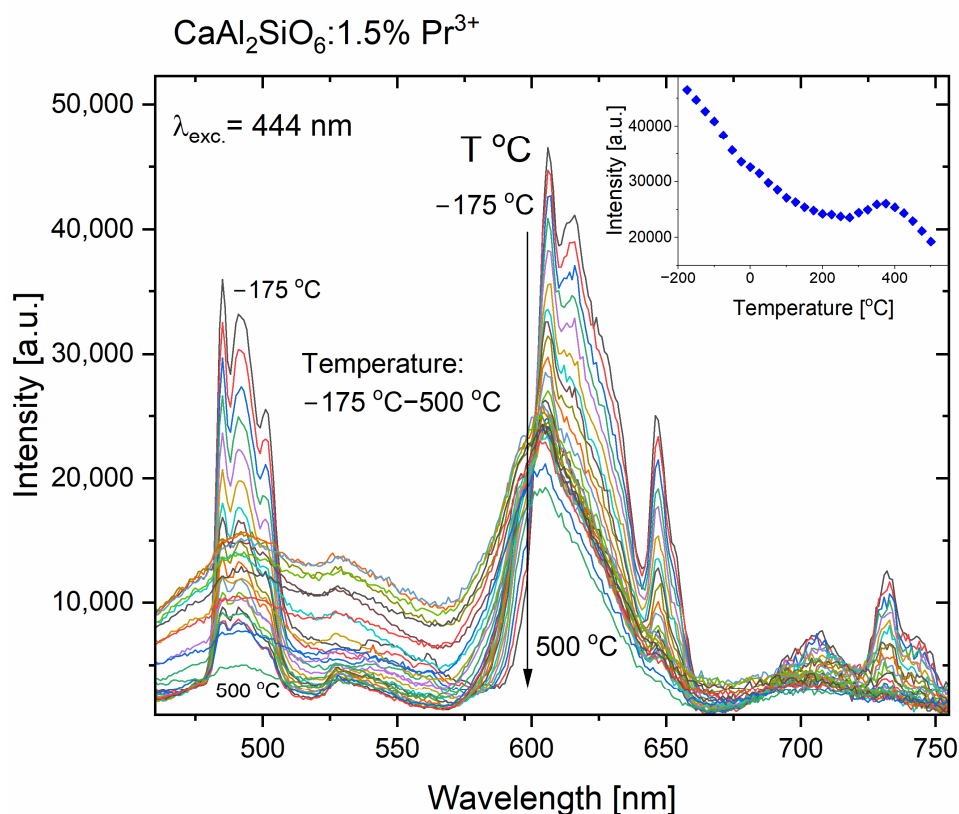


Figure 7. Temperature-dependent emission spectra of the $\text{CaAl}_2\text{SiO}_6:\text{Pr}^{3+}$ polycrystals. Inset presents the intensity values of the $^1\text{D}_2 \rightarrow ^3\text{H}_4$ emission in $\text{CaAl}_2\text{SiO}_6:\text{Pr}^{3+}$, changing with the increasing temperature.

Thermal quenching was described as a thermally activated process with an activation energy ΔE , which was performed by fitting the Arrhenius equation [36,37]:

$$I(T) = \frac{I_0}{1 + Ae^{-\Delta E/kT}}, \quad (1)$$

where I_0 is the initial emission intensity of the $\text{CaAl}_2\text{SiO}_6:\text{Pr}^{3+}$ at the lowest temperature of -175°C , $I(T)$ is the intensity at different temperatures, A is a constant, k is the Boltzmann constant, and T is the temperature of the sample. Figure 8 presents the fit line of the thermal quenching emission model plotted as $\ln((I_0/I) - 1)$ against $1/k$. Based on the Arrhenius equation (Equation (1)), the value of the activation energy for thermal quenching ΔE of this compound was calculated to be 0.044 eV, which gives the energy value of 355 cm^{-1} . This is sufficient for electrons to move from the $^3\text{P}_0$ to the $^3\text{P}_1$ energy level, which quenches the emission coming from the $^3\text{P}_0$ level.

The results of the luminescence lifetime kinetics measurements are presented in Figure 9 for the $^1\text{D}_2$ emitting level of Pr^{3+} . The luminescence decay curves have a non-exponential character. The average emission lifetime was determined using the integral formula [38]. The obtained results of $^3\text{P}_0 \rightarrow ^3\text{H}_4$ emission in $\text{CaAl}_2\text{SiO}_6:\text{Pr}^{3+}$ are about 5–6 microseconds for all samples. The longest $^1\text{D}_2 \rightarrow ^3\text{H}_4$ emission lifetime of 370 milliseconds is possessed by the sample with the lowest concentration of Pr^{3+} ions, 0.1%. Samples containing higher Pr^{3+} concentrations have smaller, similar luminescence lifetime values. This may be due to the valence mismatch between Pr^{3+} and Ca^{2+} ions, and non-radiative processes between Pr^{3+} ions, such as energy migration and cross-relaxation processes, leading to the concentration quenching, even for relatively low amounts of Pr^{3+} dopant.

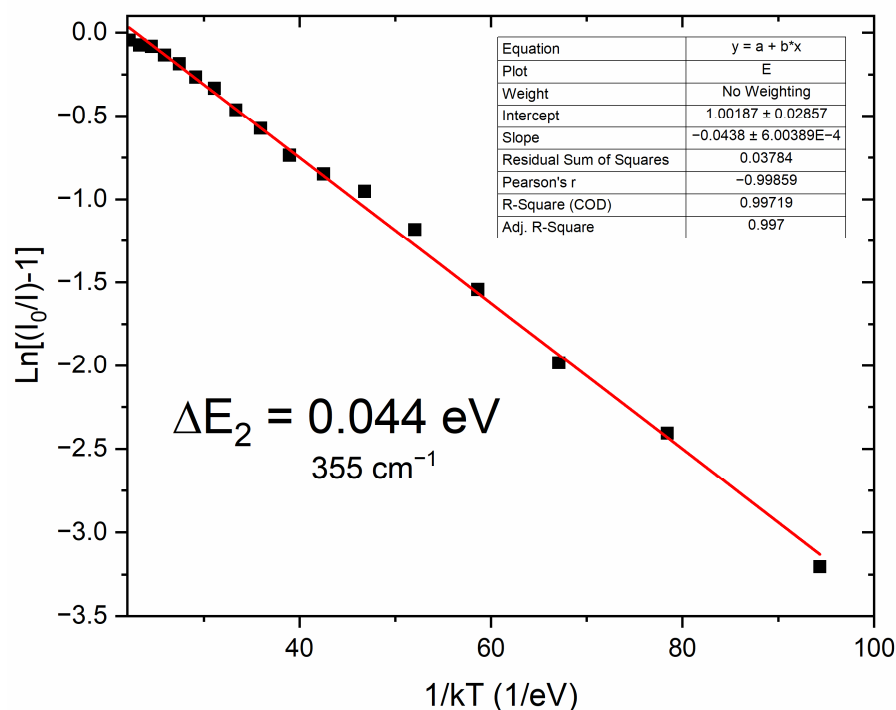


Figure 8. The activation energy of the thermal quenching, fitted using the Arrhenius equation for $\text{CaAl}_2\text{SiO}_6:1.5\% \text{Pr}^{3+}$ polycrystals.

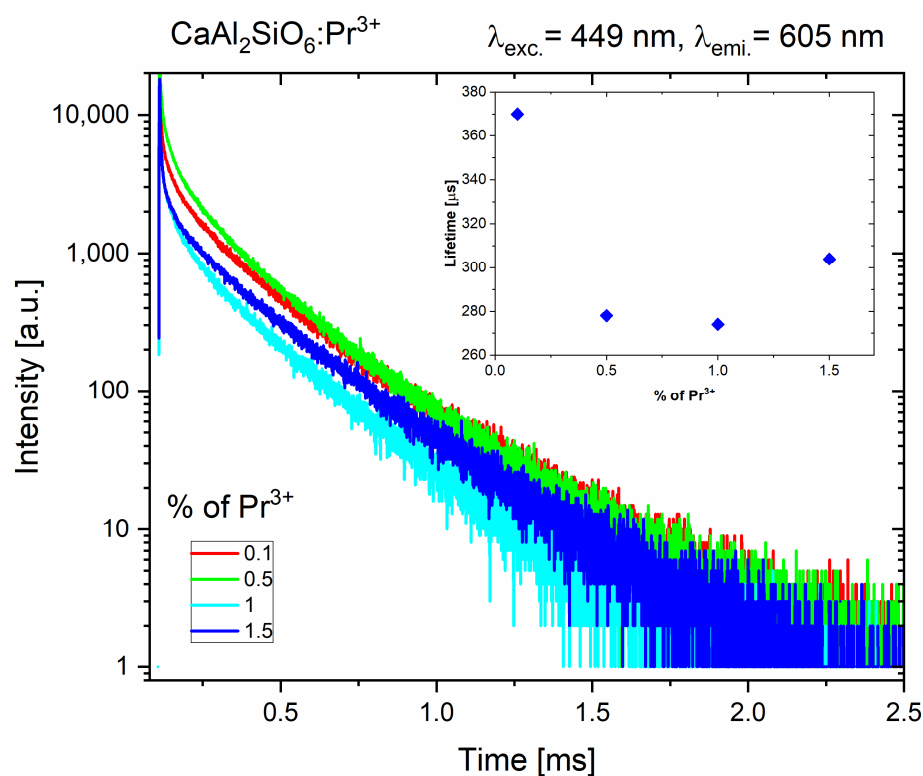


Figure 9. Luminescence decay curves and the obtained emission lifetimes values (inset) of the $^1\text{D}_2 \rightarrow ^3\text{H}_4$ emission in $\text{CaAl}_2\text{SiO}_6:\text{Pr}^{3+}$.

The two emission bands visible in Figure 10 represent emission in the UVC region, up to 280 nm, partly also in the UVB range, between 280 and 315 nm, and also a small part in the UVA range, which is from 315 to 400 nm. The broader spectrum, in the range of about

240–370 nm, consisting of two broad bands, was excited by radiation of a deuterium lamp with a wavelength of 160 nm.

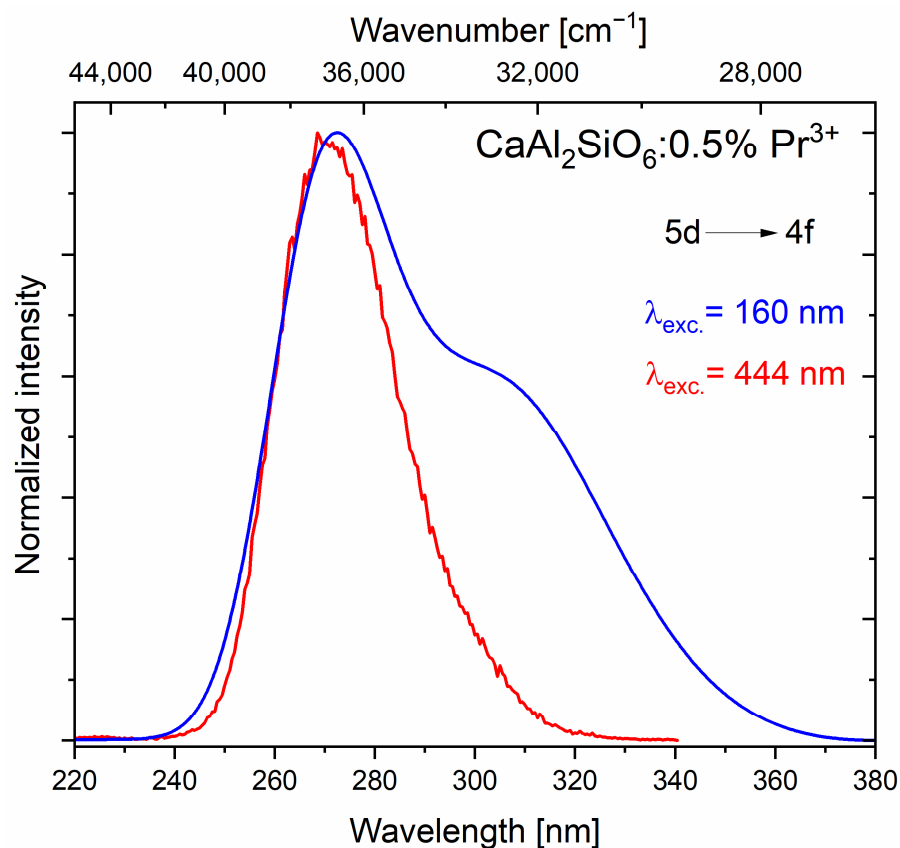


Figure 10. The 5d→4f emission in $\text{CaAl}_2\text{SiO}_6:\text{Pr}^{3+}$, obtained through the Stokes (blue spectrum) and anti-Stokes (red spectrum) processes.

The second, narrower emission band in the range of 240–330 nm visible in the figure was recorded using a blue laser operating at 444 nm. These spectra are identical, and the visible differences result from the use of different detectors. In the upconversion measurements, a photomultiplier (R7154P Hamamatsu, Hamamatsu City, Shizuoka Pref., Japan) adapted to the UV range, the so-called “solar blind”, was used so that the sample could be excited by a laser from the visible range without interfering with the measurement. In the range above 300 nm, the sensitivity of this photomultiplier drops rapidly, so the second band, located closer to the visible range, is “invisible” for this measurement. The peak of the more intense band is located at the wavenumber equal to $36,649\text{ cm}^{-1}$, while for the second band, it is at $32,465\text{ cm}^{-1}$ (with Stokes excitation, radiation of wavelength 160 nm). The difference between the peaks of these bands defined in this way is 4184 cm^{-1} , which corresponds to the difference between the levels of the $^3\text{H}_6$ and $^3\text{H}_4$ multiplets, 5d→4f transitions for Pr^{3+} ions.

The mechanisms of the most important radiative processes are visualized on the energy level diagram for the praseodymium (III) ions (Figure 11). Blue radiation (e.g., at 444 nm, which is equal to $22,523\text{ cm}^{-1}$) pumps the $^3\text{P}_J$ energy levels; then, mainly the $^3\text{P}_0$ level emits blue, green, or red radiation. The blue radiation can also involve the upconversion process, where two lower-energy photons give one high-energy photon, from the 5d energy level, in the ultraviolet region.

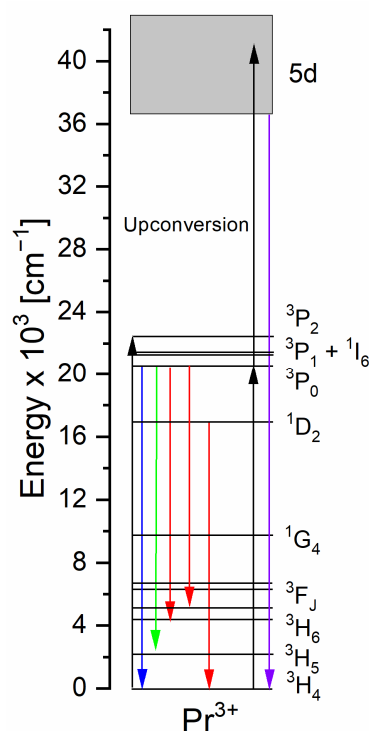


Figure 11. The excitation and emission mechanisms for the Pr^{3+} ions.

The results of the intensity of the anti-Stokes emission, excited by a blue laser at 444 nm and monitored at a wavelength of 270.5 nm, i.e., in the UVC region, are shown in Figure 12. With the increase in the Pr^{3+} ion content in the CASO matrix, the luminescence intensity increases due to the increase in the number of emission centers, with a maximum of 1% Pr^{3+} content. However, for a larger amount, 1.5% Pr^{3+} , the intensity decreases due to non-radiative parasitic effects, which contribute to the luminescence quenching.

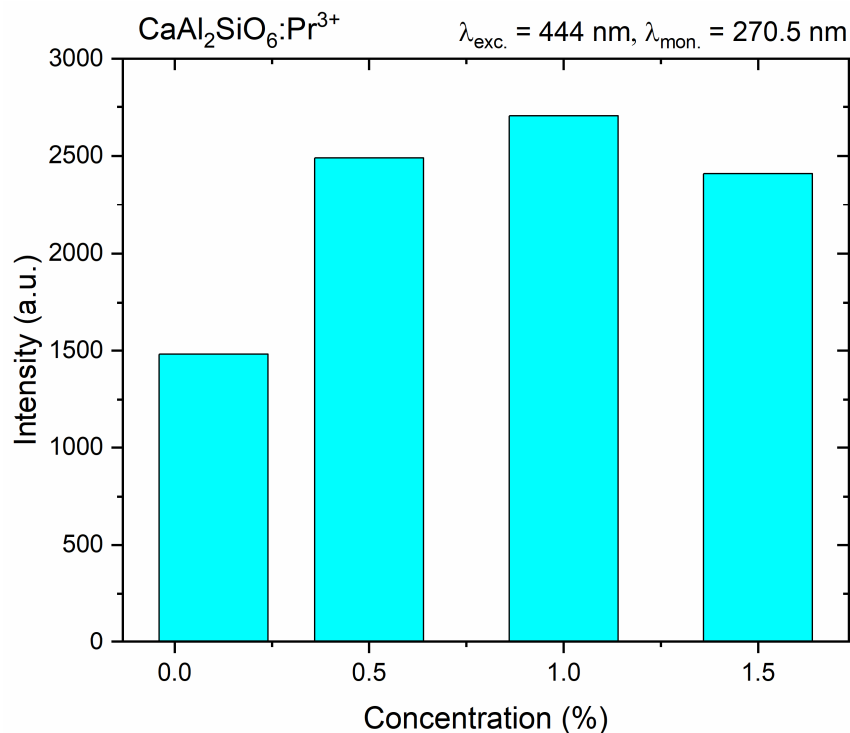


Figure 12. The visualization of the 5d → 4f emission intensity obtained through the upconversion process for $\text{CaAl}_2\text{SiO}_6:\text{Pr}^{3+}$ samples.

For the obtained upconversion in the UVC region, the influence of the laser radiation power density on the intensity of this emission was examined (Figure 13). This characteristic is in the log/log scale, because it is proportional to $I \sim P^n$ [39], where I is intensity, P is laser power and n is a number of the pump photons required to excite the emitting level. The obtained characteristic can be fitted by the linear function, and $n = 1.9$, which means that two photons are involved in this process.

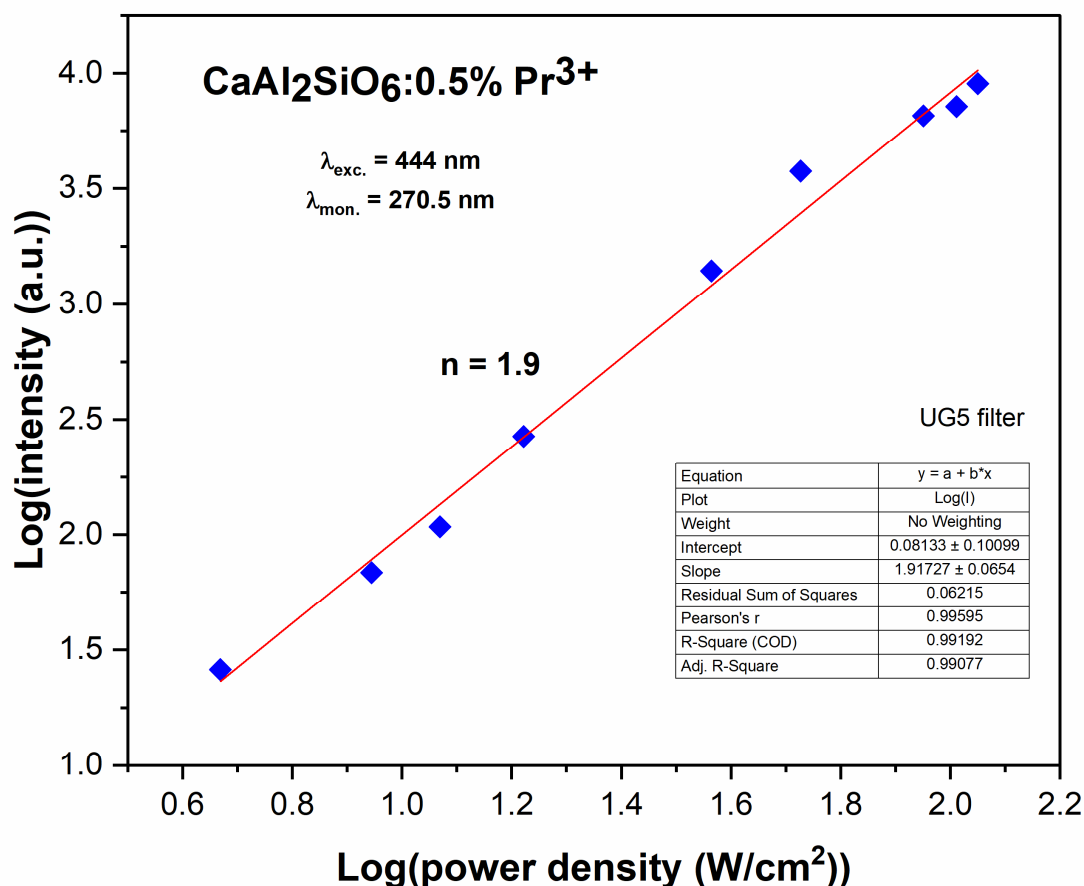


Figure 13. Power density dependence on the intensity of the 5d→4f upconversion emission for $\text{CaAl}_2\text{SiO}_6:\text{Pr}^{3+}$ (excitation wavelength is 444 nm, and the monitored wavelength is 270.5 nm).

The emission and excitation spectra of $\text{CaAl}_2\text{SiO}_6:1.5\% \text{Pr}^{3+}$ crystallites, obtained using synchrotron radiation, are characteristic of other Pr^{3+} -activated silicate hosts [40] (Figure 14). The bands in the excitation spectrum from 150 to 270 nm correspond to the $4f^2 \rightarrow 5d^1 4f^1$ transition of the praseodymium ion [41]. Under 188 nm excitation, the emission spectrum is dominated in the 230–350 nm range, corresponding to the transition from $5d4f$ to $^3\text{H}_j$ and $^3\text{F}_j$ [42]. Additionally, the emission spectrum features a band with a maximum at 490 nm, attributed to the $^3\text{P}_0 \rightarrow ^3\text{H}_4$ transition of Pr^{3+} . This occurs as a result of a non-radiative transition from the 5d electron configuration to the f configuration, often associated with significant Stokes shifts (ΔS) exceeding 3000 cm^{-1} [43]. However, according to theoretical predictions, the ideal hosts for blue-to-UVC upconversion should have a Stokes shift of less than 3000 cm^{-1} [44,45].

Based on the lowest-energy f–d excitation bands and the highest-energy d–f emission maxima (E_{em}), the Stokes shift (ΔS) for CASO was determined to be 3400 cm^{-1} , explaining the observed emission in the visible region of the spectrum. Nevertheless, in CASO, the

lowest energy level of $4f^15d^1$ for Pr^{3+} is quite low, namely $38,287\text{ cm}^{-1}$. This value was calculated using the following equation [20,46]:

$$E_{fd} = E_{em} + 1/2\Delta S, \quad (2)$$

where E_{fd} is the lowest energy level. As a result, in the upconversion mechanism under 444 nm ($22,522\text{ cm}^{-1}$) excitation, not only the $^3\text{P}_0$ level but also the $^1\text{D}_2$ level serve as intermediate states, making $\text{CaAl}_2\text{SiO}_6$ a prospective matrix for practical application.

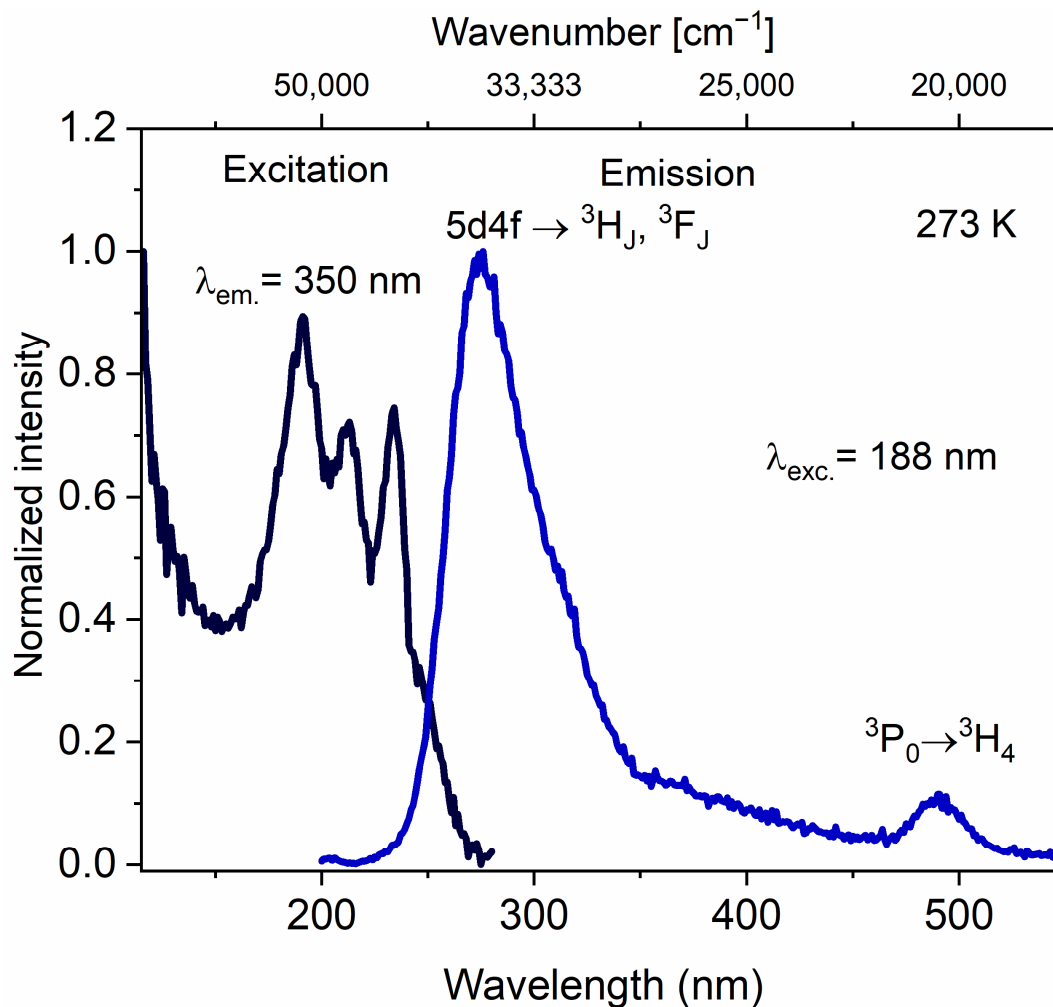


Figure 14. Excitation ($\lambda_{em.} = 350\text{ nm}$) and emission ($\lambda_{exc.} = 188\text{ nm}$) spectra of $\text{CaAl}_2\text{SiO}_6:1.5\%\text{Pr}^{3+}$ using synchrotron radiation.

The primary mechanism responsible for the luminescence of the praseodymium ion from the visible to the ultraviolet region is most often excited state absorption (ESA) [47,48]. All the decay profiles exhibit an additional peak of around 250 ns, attributed to a phenomenon known as ringing, which is common in this type of measurement [49,50]. The upconversion lifetime of the CASO phosphor was studied under excitation by a 443.4 nm pulsed laser (Figure 15). The upconversion decay time constants were determined based on the integral formula. The obtained decay times range from 24 to 21 ns, which is approximately equal to the 5d luminescence lifetime of the praseodymium ion [51]. The ESA mechanism is confirmed as the dominant process responsible for upconversion in this case.

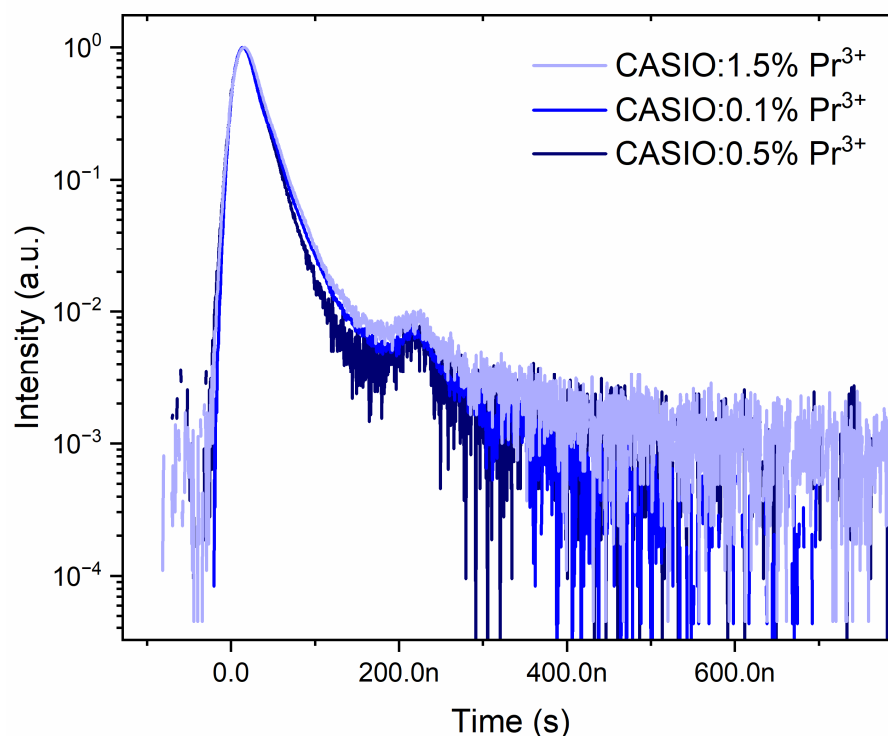
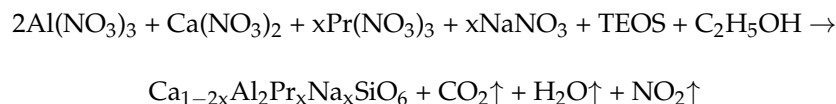


Figure 15. Decay profiles of upconversion emission under 443.4 nm pulsed excitation of $\text{CaAl}_2\text{SiO}_6:\text{xPr}^{3+}$.

3. Materials and Methods

3.1. Synthesis

$\text{CaAl}_2\text{SiO}_6:\text{Pr}^{3+}$ nanoparticles were synthesized by the sol–gel method. Since the Pr^{3+} ion is close in size to the Ca^{2+} ion, it occupies the calcium position in the crystal lattice of $\text{CaAl}_2\text{SiO}_6$. To balance the charge, an appropriate amount of sodium ions was added to the aluminosilicate composition. The starting materials $\text{Ca}(\text{NO}_3)_2 \cdot 4\text{H}_2\text{O}$ (99%, Alfa Aesar, Haverhill, MA, USA), $\text{Al}(\text{NO}_3)_3 \cdot 9\text{H}_2\text{O}$ (99.999%, Sigma Aldrich, St. Louis, MO, USA), NaNO_3 (99.8%, Sigma Aldrich, St. Louis, MO, USA), and $\text{Pr}(\text{NO}_3)_3 \cdot 6\text{H}_2\text{O}$ (99.99%, Alfa Aesar, Haverhill, MA, USA) were dissolved in a mixture of 5 mL ethanol and 10 mL deionized water. The resulting clear solution was slowly poured into a stoichiometric amount of TEOS ($\text{Si}(\text{OC}_2\text{H}_5)_4$) (99%, Sigma Aldrich, St. Louis, MO, USA) with vigorous stirring. The solution remained clear and gave no precipitate during the stirring process for 2 h at room temperature. To evaporate the solvent, the mixture was heated at 70 °C for 24 h. The resulting viscous gel was heated at a rate of 5 °C/min in an ambient atmosphere to 500 °C for 3 h then cooled to room temperature, ground in an agate mortar, and calcined at 1000 °C for 10 h. The following scheme shows the synthesis process:



3.2. Measurements

X-ray powder diffraction (XRPD) measurements were collected using an X'Pert PRO X-ray diffractometer (Panalytical, Malvern, UK). The absorption spectra were recorded using a Cary 5000 UV-VIS-NIR spectrophotometer (Agilent Technologies, Santa Clara, CA, USA). Excitation, emission spectra, and decay time profiles were measured using an FLS1000 fluorescence spectrometer (Edinburgh Instruments, Livingston, UK), equipped with a

450 W xenon lamp. Emission characteristics were also determined using a femtosecond laser (Coherent Model “Libra”) that delivers a train of 100 fs pulses at a center wavelength of 800 nm and pulse energy up to 1 mJ with a repetition rate regulated up to 1 kHz. The lifetime of the short-living 3P_0 level was obtained using the picosecond pulsed laser diode, operating at 450 nm. For the temperature-dependent emission spectra, the Hamamatsu (Hamamatsu City, Shizuoka Pref., Japan) PMA-12 detector with Linkam (Salfords, UK) THMS 600 Heating/Freezing Stage and a laser at 444 nm was used. Measurements in the UVC region were performed using a VUV McPherson spectrometer (McPherson, Chelmsford, MA, USA), equipped with a 150 W deuterium lamp. The upconversion emission was recorded on the McPherson spectrometer, using the excitation laser line at 444 nm. Excitation and emission spectra in ultraviolet range (in Figure 14) were recorded at SUPERLUMI (DESY, Germany) using a 2-meter McPherson monochromator and a Hamamatsu R6836 photomultiplier.

4. Conclusions

The new compounds of nanocrystalline $\text{CaAl}_2\text{SiO}_6\text{:Pr}^{3+}$ aluminosilicates have been synthesized and measured for the first time. The investigation of the spectroscopic properties indicates that the blue, green, and red Stokes emissions of the Pr^{3+} occur in this crystal host. The Stokes emission in the visible range is observed mainly from the 3P_0 or 1D_2 energy levels to the ground state 3H_4 . The red emission of $^1D_2 \rightarrow ^3H_4$ is very stable even at very high temperatures.

The $5d \rightarrow 4f$ transition, mainly in the UVC but also in the UVB and UVA range, is observed by high-energy excitation in the UV range (Stokes emission) and by lower-energy excitation with visible light in the blue range (anti-Stokes emission). The UVC $5d \rightarrow 4f$ emission is much stronger than the $4f \rightarrow 4f$ luminescence. This is caused by the fact that the majority of the excitation energy is transferred directly to the 5d band, which does not lose much of this energy for transfer to the 4f praseodymium levels. Therefore, the UVC emission from the 5d level of Pr^{3+} ions in the $\text{CaAl}_2\text{SiO}_6$ matrix is much more efficient.

The investigated compounds are potentially useful for human health applications, because they possess characteristics that confirm their potential for upconversion emission in the UV range for disinfection purposes, to successfully destroy viruses and bacteria.

Author Contributions: Conceptualization, K.L. and P.J.D.; methodology, K.L., N.R. and P.Z.-S.; validation, K.L., N.R. and P.J.D.; formal analysis, K.L. and P.J.D.; investigation, K.L., N.R. and P.Z.-S.; resources, N.R. and P.J.D.; data curation, K.L. and N.R.; writing—original draft, K.L. and N.R.; writing—review and editing, K.L., P.J.D. and N.R.; visualization, K.L. and N.R.; supervision, K.L. and P.J.D. All authors have read and agreed to the published version of the manuscript.

Funding: This research was funded by the National Science Centre (NCN) under the OPUS 21 project, grant no. UMO-2021/41/B/ST5/03792, which is gratefully acknowledged.

Institutional Review Board Statement: Not applicable.

Informed Consent Statement: Not applicable.

Data Availability Statement: The data presented in this study are available on request from the corresponding author.

Acknowledgments: The investigation using synchrotron radiation at the P66 SUPERLUMI station at DESY, Hamburg, Germany was performed within the framework of I-20240194 EC project. The authors would like to thank Robert Kowalski for the measurements on the femtosecond laser and Jarosław Komar for help with the measurements made on the FLS1000 spectrometer.

Conflicts of Interest: The authors declare no conflicts of interest.

References

- Bloembergen, N. Solid State Infrared Quantum Counters. *Phys. Rev. Lett.* **1959**, *2*, 84–85. [\[CrossRef\]](#)
- Auzel, F. Compteur Quantique Par Transfert d'énergie Entre Deux Ions de Terres Rares Dans Un Tungstate Mixte et Dans Un Verre. *CR Acad. Sci. Paris* **1966**, *262*, 1016–1019.
- Auzel, F.E. Materials and Devices Using Double-Pumped-Phosphors with Energy Transfer. *Proc. IEEE* **1973**, *61*, 758–786. [\[CrossRef\]](#)
- Blasse, G.; Grabmaier, B.C. *Luminescent Materials*; Springer: Berlin/Heidelberg, Germany, 1994; ISBN 978-3-540-58019-5.
- Lemański, K.; Pazik, R.; Dereń, P.J. Efficient Up-Conversion Emission and Energy Transfer in LaAlO₃ Doped with Er³⁺, Ho³⁺, and Yb³⁺ Ions. *Opt. Mater.* **2012**, *34*, 1990–1993. [\[CrossRef\]](#)
- Marciniak, L.; Stefanski, M.; Tomala, R.; Hreniak, D.; Strek, W. Synthesis and Up-Conversion Luminescence of Er³⁺ and Y B³⁺ Codoped Nanocrystalline Tetra- (KLaP₄O₁₂) and Pentaphosphates (LaP₅O₁₄). *J. Chem. Phys.* **2015**, *143*, 094701. [\[CrossRef\]](#)
- Pilch, A.; Wawrzyńczyk, D.; Kurnatowska, M.; Czaban, B.; Samoć, M.; Strek, W.; Bednarkiewicz, A. The Concentration Dependent Up-Conversion Luminescence of Ho³⁺ and Yb³⁺ Co-Doped β-NaYF₄. *J. Lumin.* **2017**, *182*, 114–122. [\[CrossRef\]](#)
- Runowski, M.; Shyichuk, A.; Tymiński, A.; Grzyb, T.; Lavín, V.; Lis, S. Multifunctional Optical Sensors for Nanomanometry and Nanothermometry: High-Pressure and High-Temperature Upconversion Luminescence of Lanthanide-Doped Phosphates—LaPO₄/YPO₄:Yb³⁺–Tm³⁺. *ACS Appl. Mater. Interfaces* **2018**, *10*, 17269–17279. [\[CrossRef\]](#)
- Hölsä, J.; Laihin, T.; Laamanen, T.; Lastusaari, M.; Pihlgren, L.; Rodrigues, L.C.V.; Soukka, T. Enhancement of the Up-Conversion Luminescence from NaYF₄:Yb³⁺, Tb³⁺. *Phys. B Condens. Matter* **2014**, *439*, 20–23. [\[CrossRef\]](#)
- Naccache, R.; Vetrone, F.; Speghini, A.; Bettinelli, M.; Capobianco, J.A. Cross-Relaxation and Upconversion Processes in Pr³⁺ Singly Doped and Pr³⁺/Yb³⁺ Codoped Nanocrystalline Gd₃Ga₅O₁₂: The Sensitizer/Activator Relationship. *J. Phys. Chem. C* **2008**, *112*, 7750–7756. [\[CrossRef\]](#)
- Guyot, Y.; Moncorgé, R.; Merkle, L.D.; Pinto, A.; McIntosh, B.; Verdun, H. Luminescence Properties of Y₂O₃ Single Crystals Doped with Pr³⁺ or Tm³⁺ and Codoped with Yb³⁺, Tb³⁺ or Ho³⁺ Ions. *Opt. Mater.* **1996**, *5*, 127–136. [\[CrossRef\]](#)
- Dramićanin, M.D.; Brik, M.G.; Antić, Ž.; Bănică, R.; Mosoarca, C.; Dramićanin, T.; Ristić, Z.; Dima, G.D.; Förster, T.; Suta, M. Pr³⁺ Visible to Ultraviolet Upconversion for Antimicrobial Applications. *Nanomaterials* **2025**, *15*, 562. [\[CrossRef\]](#) [\[PubMed\]](#)
- Aboamer, M.A.; Alsuaayri, A.S.; Alassaf, A.; Alqahtani, T.M.; Alresheedi, B.A.; Saijari, G.N.; Osman, E.A.; Mohamed, N.A.R. Hybrid Radiant Disinfection: Exploring UVC and UVB Sterilization Impact on the Mechanical Characteristics of PLA Materials. *Polymers* **2023**, *15*, 4658. [\[CrossRef\]](#) [\[PubMed\]](#)
- Hamamoto, A.; Mori, M.; Takahashi, A.; Nakano, M.; Wakikawa, N.; Akutagawa, M.; Ikehara, T.; Nakaya, Y.; Kinouchi, Y. New Water Disinfection System Using UVA Light-emitting Diodes. *J. Appl. Microbiol.* **2007**, *103*, 2291–2298. [\[CrossRef\]](#)
- Nakahashi, M.; Mawatari, K.; Hirata, A.; Maetani, M.; Shimohata, T.; Uebanso, T.; Hamada, Y.; Akutagawa, M.; Kinouchi, Y.; Takahashi, A. Simultaneous Irradiation with Different Wavelengths of Ultraviolet Light Has Synergistic Bactericidal Effect on *Vibrio parahaemolyticus*. *Photochem. Photobiol* **2014**, *90*, 1397–1403. [\[CrossRef\]](#)
- Lemański, K.; Bondzior, B.; Szymański, D.; Dereń, P.J. Spectroscopic Properties of Gd_xLa_{1-x}AlO₃ Nanocrystals Doped with Pr³⁺ Ions. *New J. Chem.* **2019**, *43*, 6242–6248. [\[CrossRef\]](#)
- Macalik, B.; Lisiecki, R.; Kowalski, R.M.; Ryba-Romanowski, W. Down- and up-Conversion of Femtosecond Light Pulses into Pr³⁺ Luminescence in LiTaO₃:Pr³⁺ Single Crystal. *J. Lumin.* **2020**, *224*, 117294. [\[CrossRef\]](#)
- Zhanturina, N.; Beketova, G.; Gorecka, N.; Szczodrowski, K.; Lesniewski, T.; Aimaganbetova, Z.; Bizhanova, K.; Bekeshev, A. Luminescence Properties of LaAlO₃:Pr under Hydrostatic Pressure. *Crystals* **2023**, *13*, 1558. [\[CrossRef\]](#)
- Lemański, K.; Bezukrovna, O.; Rebrova, N.; Lisiecki, R.; Zdeb, P.; Dereń, P.J. UVC Stokes and Anti-Stokes Emission of Ca₉Y(PO₄)₇ Polycrystals Doped with Pr³⁺ Ions. *Molecules* **2024**, *29*, 2084. [\[CrossRef\]](#)
- Rebrova, N.; Zdeb, P.; Lemański, K.; Macalik, B.; Bezukrovnyi, O.; Dereń, P.J. Upconversion Luminescence Properties of Pr³⁺-Doped BaYF₅ Nanoparticles Prepared by Microwave Hydrothermal Method. *Inorg. Chem.* **2024**, *63*, 3028–3036. [\[CrossRef\]](#)
- Weber, M.J. Multiphonon Relaxation of Rare-Earth Ions in Yttrium Orthoaluminate. *Phys. Rev. B* **1973**, *8*, 54–64. [\[CrossRef\]](#)
- Dereń, P.J.; Mahiou, R.; Goldner, P. Multiphonon Transitions in LaAlO₃ Doped with Rare Earth Ions. *Opt. Mater.* **2009**, *31*, 465–469. [\[CrossRef\]](#)
- Vaniman, D.T.; Bish, D.L. Yoshiokaite, a New Ca,Al-Silicate Mineral from the Moon. *Am. Mineral.* **1990**, *75*, 676–686.
- Lemański, K.; Walerczyk, W.; Dereń, P.J. Luminescent Properties of Europium Ions in CaAl₂SiO₆. *J. Alloys Compd.* **2016**, *672*, 595–599. [\[CrossRef\]](#)
- Lemański, K. Tunable Phosphor Properties of the CaAl₂SiO₆ Polycrystals Doped with Chromium, Manganese and Vanadium Ions. *Solid State Sci.* **2023**, *144*, 107300. [\[CrossRef\]](#)
- Lemański, K. Optical Properties of CaAl₂SiO₆ Polycrystals Doped with Ce³⁺ and Nd³⁺ Ions. *Bull. Mater. Sci.* **2024**, *47*, 70. [\[CrossRef\]](#)
- Wang, B.; Sun, L.; Ju, H. Luminescence and Energy Transfer of White-Light Emitting CaAl₂SiO₆:Ce³⁺, Tb³⁺ Phosphors. *Solid State Commun.* **2010**, *150*, 1460–1462. [\[CrossRef\]](#)

28. Sun, L.; Wang, B.; Ju, H.; Xu, S. Optical Properties of $\text{CaAl}_2\text{SiO}_6$: Eu^{2+} Phosphors Prepared by a Sol-Gel Method. *J. China Jiliang Univ.* **2008**, *19*, 372.
29. Steele, I.M.; Pluth, J.J. Crystal Structure of Synthetic Yoshiokaite, a Stuffed Derivative of the Tridymite Structure. *Am. Mineral.* **1990**, *75*, 1186–1191.
30. Shannon, R.D. Revised Effective Ionic Radii and Systematic Studies of Interatomic Distances in Halides and Chalcogenides. *Acta Crystallogr. Sect. A* **1976**, *32*, 751–767. [[CrossRef](#)]
31. Williamson, G.K.; Hall, W.H. X-Ray Line Broadening from Filled Aluminium and Wolfram. *Acta Metall.* **1953**, *1*, 22–31. [[CrossRef](#)]
32. Scherrer, P. Bestimmung Der Grösse Und Der Inneren Struktur von Kolloidteilchen Mittels Röntgenstrahlen. *Nachrichten Ges. Wiss. Göttingen Math.-Phys. Kl.* **1918**, *1918*, 98–100.
33. Korotkov, A.S.; Atuchin, V.V. Prediction of Forbidden Band Gap of Oxide Crystal by Chemical Formula. In Proceedings of the 2008 9th International Workshop and Tutorials on Electron Devices and Materials, Novosibirsk, Russia, 1–5 July 2008; IEEE: New York, NY, USA, 2008; pp. 23–25.
34. Lemański, K.; Babij, M. Tunable Spectroscopic Properties of Benitoite $\text{BaTiSi}_2\text{GeO}_9$: Eu^{3+} Phosphors. *Mater. Res. Bull.* **2024**, *180*, 113035. [[CrossRef](#)]
35. Guan, Y.; Tsuboi, T.; Huang, Y.; Huang, W. Concentration Quenching of Praseodymium Ions Pr^{3+} in $\text{BaGd}_2(\text{MoO}_4)_4$ Crystals. *Dalton Trans.* **2014**, *43*, 3698–3703. [[CrossRef](#)] [[PubMed](#)]
36. Lemański, K.; Sztolberg, D.; Brzostowski, B.; Drzewiecki, A.; Stefańska, D.; Dereń, P.J. Spectroscopic and Paramagnetic Studies of LaAlO_3 Polycrystals Doped with Manganese Ions. *Mater. Chem. Phys.* **2020**, *250*, 123149. [[CrossRef](#)]
37. Chi, F.; Wei, X.; Jiang, B.; Chen, Y.; Duan, C.; Yin, M. Luminescence Properties and the Thermal Quenching Mechanism of Mn^{2+} Doped Zn_2GeO_4 Long Persistent Phosphors. *Dalton Trans.* **2018**, *47*, 1303–1311. [[CrossRef](#)]
38. Lemański, K.; Babij, M. Modulation of the Optical Properties of $\text{Na}_2\text{ZnGeSi}_1\text{-XO}_4$ Polycrystals Doped with Eu^{3+} Ions. *J. Lumin.* **2025**, *284*, 121316. [[CrossRef](#)]
39. Pollnau, M.; Gamelin, D.R.; Lüthi, S.R.; Güdel, H.U.; Hehlen, M.P. Power Dependence of Upconversion Luminescence in Lanthanide and Transition-Metal-Ion Systems. *Phys. Rev. B* **2000**, *61*, 3337–3346. [[CrossRef](#)]
40. Piccinelli, F.; Speghini, A.; Ivanovskikh, K.; Meijerink, A.; Ronda, C.; Bettinelli, M. UV and Visible Luminescence of Pr^{3+} Doped Oxides: New Materials. *MRS Proc.* **2008**, *1111*, 807. [[CrossRef](#)]
41. Zych, A.; Donegá, C.d.M.; Meijerink, A. Fast d–f Emission in Ce^{3+} , Pr^{3+} and Nd^{3+} Activated RbCl . *Opt. Mater.* **2011**, *33*, 347–354. [[CrossRef](#)]
42. Kappelhoff, J.; Keil, J.-N.; Kirm, M.; Makhov, V.N.; Chernenko, K.; Möller, S.; Jüstel, T. Spectroscopic Studies on Pr^{3+} Doped YPO_4 and LuPO_4 upon Vacuum Ultraviolet (VUV) and Synchrotron Radiation Excitation. *Chem. Phys.* **2022**, *562*, 111646. [[CrossRef](#)]
43. Srivastava, A.M. Aspects of Pr^{3+} Luminescence in Solids. *J. Lumin.* **2016**, *169*, 445–449. [[CrossRef](#)]
44. Li, L.; Zi, L.; Yang, F.; Feng, S.; Wang, C.; Yang, Y. Pr^{3+} -Based Visible-to-Ultraviolet Upconversion. A Minireview. *Adv. Phys. Res.* **2025**, *4*, 2400097. [[CrossRef](#)]
45. Srivastava, A.M.; Jennings, M.; Collins, J. The Interconfigurational ($4f15d1 \rightarrow 4f2$) Luminescence of Pr^{3+} in LuPO_4 , $\text{K}_3\text{Lu}(\text{PO}_4)_2$ and LiLuSiO_4 . *Opt. Mater.* **2012**, *34*, 1347–1352. [[CrossRef](#)]
46. Rebrova, N.; Grippa, A.; Zdeb-Stańczykowska, P.; Dereń, P.J. Unusually Effective Blue-to-UVC Upconversion of Pr^{3+} -Doped $\text{Sr}_3\text{Lu}(\text{PO}_4)_3$ and $\text{Ba}_3\text{Lu}(\text{PO}_4)_3$ Phosphors: A Comparative Study. *Inorg. Chem.* **2025**, *64*, 11146–11154. [[CrossRef](#)]
47. Rebrova, N.; Grippa, A.; Zdeb, P.; Dereń, P.J. Blue to UV Upconversion Properties of Pr^{3+} Doped ACaF_3 ($A = \text{K}, \text{Rb}, \text{Cs}$) Phosphors. *Scr. Mater.* **2025**, *255*, 116395. [[CrossRef](#)]
48. Rebrova, N.; Lisiecki, R.; Zdeb-Stańczykowska, P.; Zorenko, Y.; Voloshinovskii, A.; Pushak, A.; Dereń, P.J. Optical and Upconversion Properties of $\text{A}_3\text{Y}(\text{PO}_4)_3$: Pr^{3+} ($A = \text{Sr}, \text{Ba}$) Phosphors. *J. Phys. Chem. C* **2025**, *129*, 1873–1884. [[CrossRef](#)]
49. Cates, E.L.; Li, F. Balancing Intermediate State Decay Rates for Efficient Pr^{3+} Visible-to-UVC Upconversion: The Case of $\beta\text{-Y}_2\text{Si}_2\text{O}_7$: Pr^{3+} . *RSC Adv.* **2016**, *6*, 22791–22796. [[CrossRef](#)]
50. Lai, F.; Xu, X.; Shen, J.; Wang, Y.; Yan, Y.; Nie, Y.; You, W.; Wu, D.; Han, L.; Xiao, Z. Structure and Upconversion Luminescence Properties of Pr^{3+} -Doped Y_2SiO_5 Phosphor. *Silicon* **2023**, *15*, 1913–1923. [[CrossRef](#)]
51. Trevisani, M.; Ivanovskikh, K.V.; Piccinelli, F.; Bettinelli, M. Fast 5d–4f Luminescence in Pr^{3+} -Doped $\text{K}_3\text{Lu}(\text{PO}_4)_2$. *J. Lumin.* **2014**, *152*, 2–6. [[CrossRef](#)]

Disclaimer/Publisher’s Note: The statements, opinions and data contained in all publications are solely those of the individual author(s) and contributor(s) and not of MDPI and/or the editor(s). MDPI and/or the editor(s) disclaim responsibility for any injury to people or property resulting from any ideas, methods, instructions or products referred to in the content.